



## TRPM7 channel inhibition attenuates rheumatoid arthritis articular chondrocyte ferroptosis by suppression of the PKC $\alpha$ -NOX4 axis

Renpeng Zhou<sup>a,b,1</sup>, Yong Chen<sup>a,1</sup>, Shufang Li<sup>a</sup>, Xin Wei<sup>c</sup>, Weirong Hu<sup>d</sup>, Su'an Tang<sup>e</sup>, Jie Ding<sup>a</sup>, Wanjin Fu<sup>a</sup>, Hailin Zhang<sup>a,d</sup>, Fan Chen<sup>a,d</sup>, Wenjuan Hao<sup>a,d</sup>, Yi Lin<sup>a,d</sup>, Rendu Zhu<sup>a,d</sup>, Ke Wang<sup>d</sup>, Lei Dong<sup>a,d</sup>, Yingjie Zhao<sup>a,b</sup>, Xiaowen Feng<sup>d</sup>, Feihu Chen<sup>d</sup>, Changhai Ding<sup>e,f,\*\*</sup>, Wei Hu<sup>a,b,\*</sup>

<sup>a</sup> Department of Clinical Pharmacology, The Second Hospital of Anhui Medical University, Hefei, 230601, China

<sup>b</sup> The Key Laboratory of Anti-inflammatory and Immune Medicine, Anhui Medical University, Ministry of Education, Hefei, 230032, China

<sup>c</sup> The First Affiliated Hospital of USTC, Division of Life Sciences and Medicine, University of Science and Technology of China, Hefei, 230001, PR China

<sup>d</sup> The Key Laboratory of Major Autoimmune Diseases, Anhui Institute of Innovative Drugs, School of Pharmacy, Anhui Medical University, Hefei, 230032, China

<sup>e</sup> Clinical Research Centre, Zhujiang Hospital, Southern Medical University, Guangzhou, Guangdong, China

<sup>f</sup> Menzies Institute for Medical Research, University of Tasmania, Hobart, Tasmania, Australia

### ARTICLE INFO

#### Keywords:

Rheumatoid arthritis

Ferroptosis

TRPM7

PKC $\alpha$

NOX4

### ABSTRACT

A role for ferroptosis in articular cartilage destruction associated with rheumatoid arthritis (RA) has not been identified. We previously reported transient receptor potential melastatin 7 (TRPM7) expression was correlated with RA cartilage destruction. Herein, we further characterized a role for TRPM7 in chondrocyte ferroptosis. The expression of TRPM7 was found to be elevated in articular chondrocytes derived from adjuvant arthritis (AA) rats, human RA patients, and cultured chondrocytes treated with the ferroptosis inducer, erastin. TRPM7 knockdown or pharmacological inhibition protected primary rat articular chondrocytes and human chondrocytes (C28/I2 cells) from ferroptosis. Moreover, TRPM7 channel activity was demonstrated to contribute to chondrocyte ferroptosis by elevation of intracellular Ca<sup>2+</sup>. Mechanistically, the PKC $\alpha$ -NOX4 axis was found to respond to stimulation with erastin, which resulted in TRPM7-mediated chondrocyte ferroptosis. Meanwhile, PKC $\alpha$  was shown to directly bind to NOX4, which could be reduced by TRPM7 channel inhibition. Adeno-associated virus 9-mediated TRPM7 silencing or TRPM7 blockade with 2-APB alleviated articular cartilage destruction in AA rats and inhibited chondrocyte ferroptosis. Collectively, both genetic and pharmacological inhibitions of TRPM7 attenuated articular cartilage damage and chondrocyte ferroptosis via the PKC $\alpha$ -NOX4 axis, suggesting that TRPM7-mediated chondrocyte ferroptosis is a promising target for the prevention and treatment of RA.

### 1. Introduction

Rheumatoid arthritis (RA) is a most common autoimmune inflammatory disorder characterized by synovial inflammation, articular cartilage destruction and bone erosion, which eventually leads to joint deformity and disability [1]. Articular cartilage is an important structural and functional unit of joints, and its integrity is necessary to the normal movement of movable joints [2]. Degeneration and damage of articular cartilage are the main causes of joint function loss in patients with RA [3]. Chondrocytes, the only cell type that comprises articular

cartilage, are embedded within the extracellular matrix wherein they maintain cartilage integrity and homeostasis [4]. Progressive death of articular chondrocytes is a dominant feature of RA, playing an important role in RA initiation and exacerbation [5,6]. Therefore, investigation of the molecular basis for articular chondrocyte death will help to understand the pathogenesis and would therefore provide for a novel therapeutic approach for treatment of RA.

Ferroptosis results from iron-dependent oxidative damage, lipid peroxidation and reactive oxygen species (ROS) production which inhibit system Xc<sup>-</sup>-dependent glutathione (GSH) biosynthesis and the

\* Corresponding author. Department of Clinical Pharmacology, The Second Hospital of Anhui Medical University, Hefei, 230601, China.

\*\* Corresponding author. Clinical Research Centre, Zhujiang Hospital, Southern Medical University, Guangzhou, Guangdong, China.

E-mail addresses: [Changhai.Ding@utas.edu.au](mailto:Changhai.Ding@utas.edu.au) (C. Ding), [huwei@ahmu.edu.cn](mailto:huwei@ahmu.edu.cn) (W. Hu).

<sup>1</sup> These authors contributed equally: Renpeng Zhou, Yong Chen.

glutathione-dependent antioxidant enzyme glutathione peroxidase 4 (GPX4) [7]. Oxidative stress characterized by the overproduction of ROS is a pivotal element to trigger mitochondrial dysfunction [8]. Particularly, oxidative stress-induced depletion of mitochondrial GSH pool diminishes mitochondria function and leads to mitochondrial lipid peroxidation, thereby causing ferroptosis [9]. Ferroptosis is associated with various pathological and physiological processes, including tumor suppression, ischemia-reperfusion injury and antiviral immune response [10]. Emerging studies reported that promoting ferroptosis reduced abnormal proliferation of synovial fibroblasts and synovium inflammation, suggesting a role for ferroptosis in the pathogenesis of RA [11–13]. However, knowledge regarding the role and precise regulatory mechanism of ferroptosis in RA chondrocyte death have not been described.

Transient receptor potential melastatin 7 (TRPM7), a member of the melastatin-related subfamily, is widely expressed and characterized by a unique domain structure containing a cation channel and a protein kinase [14]. TRPM7 is highly permeable to cellular  $\text{Ca}^{2+}$  and  $\text{Mg}^{2+}$ , which play important roles in cell proliferation, differentiation, and cell death induced by oxidative stress [15–17]. Activated TRPM7 mediates  $\text{Ca}^{2+}$  overload and ROS accumulation, resulting in oxidative stress-induced anoxic neuronal death [18]. Moreover, increased expression of TRPM7 triggered a TRPM7-dependent  $\text{Ca}^{2+}$  overload that mediates kidney injury via the TLR4/NOX-2/ROS/NF- $\kappa$ B pathway, suggesting that TRPM7 acts as a novel target for treating inflammatory diseases [19]. Our previous study found TRPM7 to be highly expressed in the articular cartilage of rats with adjuvant arthritis (AA), and that blocking TRPM7 reduced articular cartilage injury in AA rats, suggesting that inhibition of TRPM7 may protect from articular cartilage damage [20]. Whether TRPM7 is involved in the regulation of RA articular chondrocyte ferroptosis is unknown, as is the mechanistic basis for such regulation.

In this study, we assess whether ferroptosis occurs during RA progression by evaluation of cartilage samples from RA patients and AA rats. Also, we investigate the role of TRPM7 in erastin-induced chondrocyte ferroptosis and its molecular mechanism of action by TRPM7 knockdown or pharmacological inhibition *in vitro*. To determine whether TRPM7 influences RA articular cartilage progression and chondrocyte ferroptosis *in vivo*, an adeno-associated virus carrying TRPM7 shRNA is used to treat AA rats. The results of the study demonstrate ferroptosis to contribute to RA articular cartilage destruction, and that blockade of TRPM7-regulated ferroptosis would serve as a promising treatment for RA.

## 2. Materials and methods

### 2.1. Human samples

Cartilage specimens were obtained from 7 patients who fulfilled the 2010 ACR diagnostic criteria and were undergoing joint replacement surgery, and from 5 normal subjects who were undergoing high amputation at the First Affiliated Hospital of Anhui Medical University and the Second Hospital of Anhui Medical University. The study was approved by the Clinical Research Ethics Committees of Anhui Medical University. Detailed clinical details are provided in Table S1.

### 2.2. Cell culture

Primary rat articular chondrocytes (RACs) were obtained from male Sprague-Dawley rats weighing 160–180 g purchased from the Center for Laboratory Animal Sciences at Anhui Medical University (Hefei, China). The study was approved by the Animal Ethics Committee of Anhui Medical University. The extraction and culture methods of primary RACs were referred previous publication [21]. Human C28/I2 cells were maintained in regular DMEM medium (Biological industries, Israel) supplemented with 10% FBS (Wisent, Canada) and 1% penicillin-streptomycin (Beyotime, China) and cultured at 37 °C in a 5%

$\text{CO}_2$  atmosphere.

### 2.3. Immunofluorescence staining

Cells were washed with PBS and fixed with 4% paraformaldehyde. Tissue sections were deparaffinized in xylene, and hydrated with decreasing concentrations of ethanol. Then, cells or tissue sections were permeabilized with 0.3% Triton X-100 (Solarbio, China) and blocked with BSA at room temperature, followed by the incubation of the primary antibodies overnight at 4 °C. Following, samples were further incubated with Alexa Fluor 488 or 594 secondary antibodies (ZSGB-Bio, China). Nuclei were stained with DAPI (Beyotime, China) for 5 min. Images were observed and taken by fluorescence microscope or laser scanning confocal microscope (ZEISS, Germany).

### 2.4. Calcium imaging

Rat articular chondrocytes were pre-incubated with naltriben (Tocris Bioscience, UK, 50  $\mu\text{M}$ ) or erastin (5  $\mu\text{M}$ ) for 20 min with/without 2-aminoethoxydiphenyl borate (2-APB, 100  $\mu\text{M}$ ), and then loaded with Fluo-4 AM (5  $\mu\text{M}$ ; Beyotime, China) for approximately 30 min. Calcium imaging was performed with the fluorescence microscope system MetaFluor software. Changes in intracellular  $\text{Ca}^{2+}$  concentration were estimated from fluorescence images of Fluo-4 AM (excitation at 488 nm, emission at 520  $\pm$  20 nm).

### 2.5. Western blot

Cells or cartilages were lysed on ice by RIPA buffer (Beyotime, China). Proteins were subjected to electrophoresis in 8–10% SDS-PAGE gel, shifted onto nitrocellulose membrane, followed by blocking with 5% non-fat milk, and then incubated of corresponding primary antibodies (Table S2) overnight at 4 °C. Then membranes were incubated with HRP-conjugated secondary antibodies. The protein bands were visualized by using an ECL solution (Affinity, USA) and detected with an automatic chemiluminescence imaging analysis system (Tanon, China). Western blot bands were quantified by using the Image J software.

### 2.6. Transmission electron microscopy

Fresh human or rat articular cartilages were collected and cut into 1  $\text{mm}^3$  pieces on ice immediately after the specimen was obtained. The cartilages or chondrocytes were fixed in 2.5% glutaraldehyde solution, post-fixed in 1% aqueous osmium tetroxide and dehydrated in gradual ethanol and acetone. The samples were prepared by gradient infiltration of anhydrous acetone and epoxy resin overnight, embedded in resin, and polymerized at 60 °C for 48 h. The embedded samples were cut into thick sections by ultra-micro-tome (Leica, Germany). Ultrathin sections were collected onto copper grids, stained with uranium acetate and lead citrate, and examined by transmission electron microscopy (Thermo, USA).

### 2.7. MTT assay

Cells were seeded at a density of  $5 \times 10^3$  cells/well in 96-well plates. After treatment, cells were incubated with MTT reagent (Beyotime, China) for 4 h at 37 °C in dark. Then DMSO was added into the wells to terminate reaction followed by the detection at the absorbance of 490 nm by microplate reader.

### 2.8. LDH assay

Cells were seeded at a density of  $5 \times 10^4$  cells/well in 24-well plates, then transferred 50  $\mu\text{l}$  supernatant to 96-well plates. Added 5% Triton X-100 and incubated for 30 min then transferred 50  $\mu\text{l}$  supernatant to 96-well plate again. Added corresponding detection reagent according to

Cytotoxicity Detection Kit (Roche, Basel, Switzerland), then detected at the absorbance of 492 nm and 620 nm by a microplate reader.

### 2.9. GSH, MDA, Fe<sup>2+</sup> and SOD assay

Cells were seeded at a density of  $5 \times 10^4$  cells/well in 6-well plates. Then the lysates of cells in the indicated groups were collected to determine GSH, MDA, Fe<sup>2+</sup> and SOD levels using corresponding kit (Table S3). The experiment was performed according to the manufacturer's instructions.

### 2.10. Lipid ROS analysis

To analyze lipid ROS, cells were seeded at a density of  $5 \times 10^4$  cells/well in 6-well plates. Then stained with 2  $\mu$ M ROS-sensitive probe BODIPY 581/591C11 (Invitrogen, USA) for 30 min at 37 °C. Cells were collected and analyzed by flow cytometry. Data were processed with FlowJo software.

### 2.11. Mitochondrial membrane potential analysis

The mitochondrial membrane potential ( $\Delta\Psi_m$ ) was detected by the Rhodamine123 (Rh123) fluorescence probe or 5,5',6,6'-tetrachloro-1,1', tetraethylbenzimidazolocarbo-cyanine iodide (JC-1) dye (Beyotime, China). Initially, cells were maintained with the Rh123 dye (2  $\mu$ M) or JC-1 dye (1 $\times$ ) for mitochondrial membrane staining for 30 min at 37 °C. Then washed with PBS twice and added anti-fluorescence attenuating tablet (Beyotime, China). Finally, images were observed and obtained by fluorescence microscope. The relative  $\Delta\Psi_m$  levels were evaluated by the red/green fluorescence ratio of the JC-1 dye in the mitochondria [22].

### 2.12. Co-immunoprecipitation (Co-IP)

Co-IP was performed using Classic IP/Co-IP Kit (Thermo, USA). Cells were lysed in weak lysate. Ten percent of the cell lysate was reserved as input, and incubated with either anti-PKC $\alpha$  antibody or control anti-mouse IgG (Beyotime, China) overnight. The immunocomplexes were incubated with protein A/G agarose beads, washed in lysis buffer 3 times, and eluted with SDS-PAGE Sample Loading Buffer (1 $\times$ ) boiling for 10 min at 100 °C, then analyzed by Western blot.

### 2.13. TRPM7 gene knockdown

C28/12 cells were infected with TRPM7 shRNA lentiviral vector (Table S4) for 24 h. Then stable cell lines were screened by 625 ng/mL puromycin (Sigma, USA) for 1 weeks, and maintained with 300 ng/mL of puromycin following instructions from the lentivirus manufacturer. The infection efficiency was determined by fluorescence microscope and Western blot.

### 2.14. Plasmid transfection

Gene sequences coding for NADPH oxidase 4 (NOX4) was cloned into the pEX-3 vector (GenePharma, China). Cells were transfected with pEX-3-NOX4 using Lipofectamine 3000 (Invitrogen, USA) according to the manufacturer's protocol. After 6 h transfection, the culture medium was replaced with fresh medium for additional 48 h. The efficiency of overexpression was confirmed by Western blot.

### 2.15. Generation of rat AAV9 vector and injection

The adeno-associated virus 9 (AAV9) was manufactured by Hanbio Biotechnology (Shanghai, China). The virus titer was  $1.0 \times 10^{12}$   $\mu$ g/mL. AAV9 expressing TRPM7 specific shRNA (Table S5) was injected intra-articularly [23]. Rats were received intra-articular injection with D-Luciferin potassium salt (Abcam, British) 21 days after injection

AAV9. After 20–30 min, cell signals of joint *in vivo* were monitored by bioluminescence imaging using the SPECTRAL ami HTX (Tucson, USA).

### 2.16. Micro-CT

Analysis of ankle bone mass was used by Skyscan 1172 Micro-21 CT system. The original data were reconstructed using NRecon to obtain the results, and sample drawing was performed using CTvox 4 software (Skyscan Bruker, Tuckson, USA). Bone morphometric parameters including bone density (BMD), bone volume percentage (BV/TV), bone surface density (BS/TV), trabecular thickness (Tb.Th), trabecular number (Tb.N) and trabecular bone (Tb.Sp) were measured.

### 2.17. Statistical analysis

All data were performed using at least three independent biological repeats, and presented as means  $\pm$  standard deviation (SD) or means  $\pm$  standard error of the mean (SEM). Prism 8 software program (GraphPad Software, La Jolla, USA) was used to compare the means for One-way analysis of variance (multiple groups) or t-tests (two groups). Arthritis score was analyzed with the Kruskal-Wallis's test. *P* values were less than 0.05 were considered significant.

## 3. Results

### 3.1. Enhanced ferroptosis and abnormal accumulation of TRPM7 in chondrocytes are involved in the progression of RA

Genome-wide RNA-Seq data (GSE10024, GSE12860) were merged to analyze the expression of ferroptosis-related genes (Fig. 1A). Gene set enrichment analysis (GSEA) demonstrated ferroptosis markers to be significantly enriched in cultured human chondrocytes stimulated with supernatant of synovial fibroblasts derived from RA patients (Fig. 1B). Heatmap analysis confirmed an upregulated profile of ferroptosis genes in RA groups (Fig. 1C, Table S6). Furthermore, as shown in Fig. 1D and E, canonical pathway analysis displayed ferroptosis was involved in RA progression through union analysis of two clusters. Safranin O/fast green staining and toluidine blue results indicated that the damaged articular cartilages of RA patients appeared to show a significant loss of glycosaminoglycans and proteoglycan with the rough surfaces and decreased cartilage volume, respectively. Ferroptosis-like mitochondria changes were also observed in chondrocytes embedded in RA cartilage as judged by transmission electron microscopy (TEM), showing a reduction of mitochondrial ridge and rupture of outer mitochondrial membrane (Fig. 1F). We also examined ferroptosis core regulators and TRPM7 expression and found ACSL4, NOX4, and TRPM7 to be dramatically elevated, and GPX4 to be significantly decreased in human RA cartilages (Fig. 1G and H).

To further validate the aforementioned findings, we established an adjuvant arthritis (AA) rat model. Similarly, the number of impaired mitochondria, and the levels of NOX4, COX2 and TRPM7 showed a significant increase, but GPX4 displayed a dramatic loss in the cartilage of AA rat (Fig. 1I and J). Moreover, a progressive increase in ACSL4, TRPM7 and a decrease in GPX4 and COL2A1 within rat cartilages were observed during the course of RA disease (Figs. S1A–D). These results demonstrate that the abnormal accumulation of TRPM7 and enhanced ferroptosis in chondrocytes are involved in RA progression.

### 3.2. Pharmacological inhibition of TRPM7 protects against articular chondrocyte ferroptosis *in vitro*

To further verify the involvement of TRPM7 in chondrocyte ferroptosis, we established *in vitro* models of ferroptosis in RACs and human chondrocytes (C28/12 cells) by using ferroptosis inducer erastin. Our results showed that erastin reduced cell viability, increased cytotoxicity in a time and concentration-dependent manner, and increased the

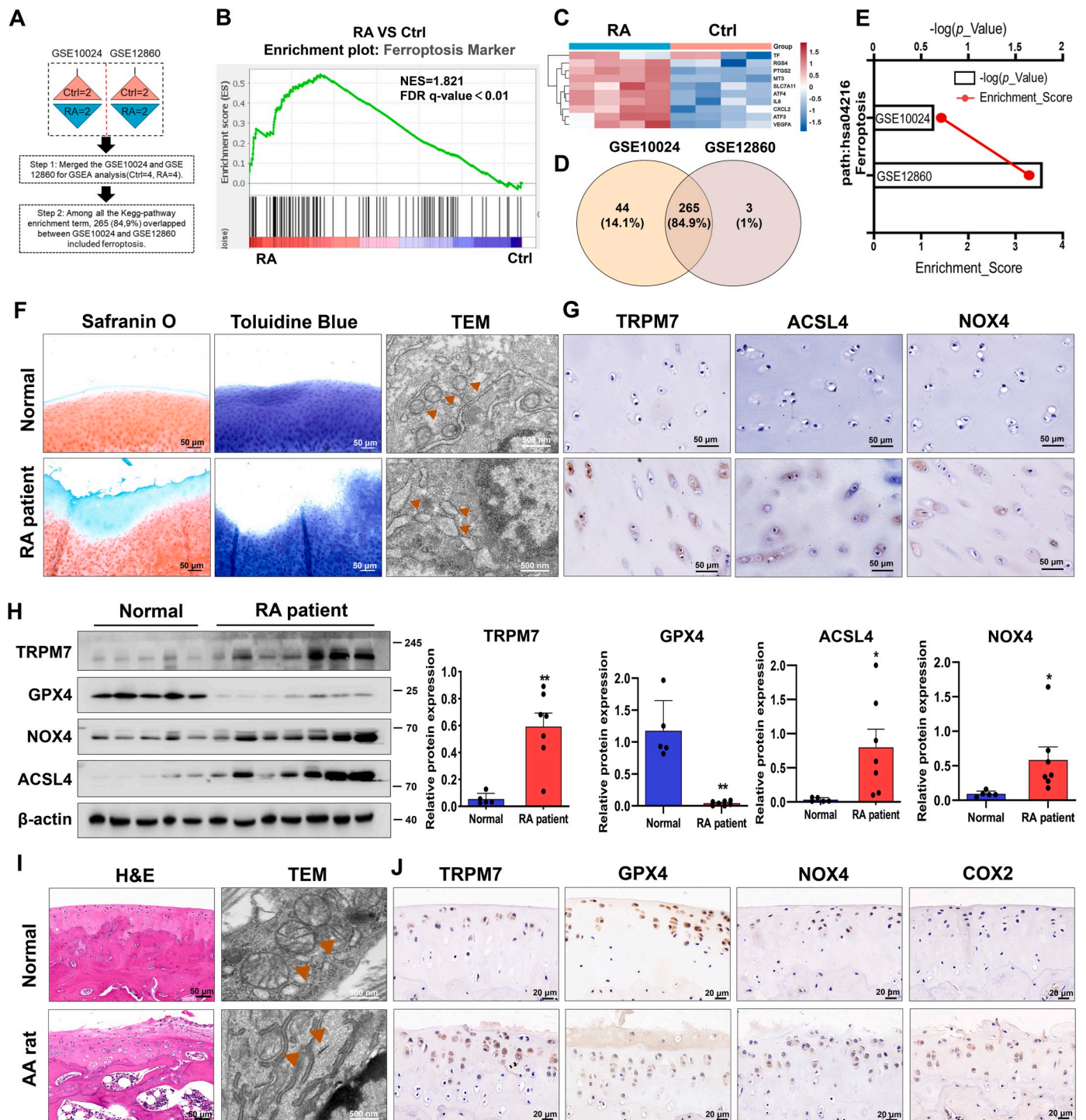


**Fig. 1.** Ferroptosis and TRPM7 in chondrocytes are tightly associated with the progression of RA. (A) Genome-wide RNA-Seq data from GSE10024 and GSE12860 (Ctrl = 4, RA = 4). (B) Gene set enrichment analysis (GSEA) and (C) heatmap analysis showing the profile of ferroptosis markers in the RA versus Ctrl group. (D) Venn diagram showing the union of two clusters (GSE10024 and GSE12860). (E) Canonical pathway analysis of GSE10024 and GSE12860. (F) Representative safranin O/ fast green staining, toluidine blue staining and TEM images of human normal and RA cartilages. Orange triangles indicate mitochondria. (G) IHC staining for TRPM7, NOX4 and ACSL4 on undamaged and RA cartilages. (H) The expression level of TRPM7 and ferroptosis-related proteins GPX4, ACSL4 and NOX4 in human normal and RA cartilages were determined by Western blot analysis (Normal = 5, RA = 7). Data are means  $\pm$  SEM. \* $P < 0.05$ , \*\* $P < 0.01$ . (I) Representative H&E staining, TEM images of cartilages from normal and AA rats ( $n = 6$  rats). Orange triangles indicate mitochondria. (J) IHC staining for TRPM7, GPX4, COX2 and NOX4 on cartilages from normal and AA rats ( $n = 6$  rats). (For interpretation of the references to colour in this figure legend, the reader is referred to the Web version of this article.)

expression of TRPM7 in RACs and C28/I2 cells, suggesting the involvement of elevated TRPM7 in ferroptosis (Fig. 2A–E). TRPM7 inhibitor 2-APB or ferroptosis inhibitor ferrostatin-1 (Fer-1) could inhibit erastin-induced chondrocyte death (Fig. 2F). Additionally, 2-APB, Fer-1 and ROS scavenger N-acetyl-L-cysteine (NAC) could restore  $\Delta\Psi_m$  to maintain mitochondrial function (Fig. 2G, Figs. S2E and F and Fig. S3E). Typical ferroptosis-like effects on mitochondria, including membrane rupture, ridge disappearance, and vacuolization were reversed by 2-APB pretreatment (Fig. 2H). In a concentration-dependent manner, 2-APB restored viability of erastin-treated chondrocytes (Fig. 2I). Further, 2-APB, Fer-1 and NAC relieved erastin-induced oxidative stress damage as judged by increased cell viability, reduced cytotoxicity, lipid-ROS production and iron overload, restored redox balance (Fig. 2J–L, Fig. S2A–D, Figs. S3A–D). In addition, ferroptosis core regulators ACSL4 and COX2 were increased, while SLC7A11, FTH and GPX4 were reduced in erastin-induced primary RACs and C28/I2 cells, which could be reversed by treatment of 2-APB, Fer-1 and NAC (Fig. 2M, N, Fig. S2G, Fig. S3G). These results demonstrate pharmacological blockade of TRPM7 could attenuate chondrocyte ferroptosis *in vitro*.

### 3.3. TRPM7 channel inhibition relieves chondrocyte ferroptosis through a $Ca^{2+}$ -dependent mechanism

To further investigate the role of genetic inhibition of TRPM7 in chondrocyte ferroptosis, two specific shRNAs were synthesized to evaluate *in vitro* knockdown of TRPM7 in C28/I2 cells (Figs. S4A and B). TRPM7 knockdown prevented human chondrocytes from erastin-induced cell death, as judged by increased cell viability, reduced cytotoxicity and restored GSH levels (Fig. 3A–C). Additionally, TEM results demonstrated that TRPM7 knockdown attenuated erastin-induced mitochondrial damage (Fig. 3B). Likewise, Western blot analysis showed that the expression of ACSL4, COX2 were reduced and SLC7A11, FTH and GPX4 were restored by TRPM7 knockdown (Fig. 3D). These results further confirm that TRPM7 deficiency negatively regulates chondrocyte ferroptosis *in vitro*.

TRPM7 is well known to have dual functions of ion channel and protein kinase [24]. However, which activity regulates articular chondrocyte ferroptosis is unknown. To determine the effects of TRPM7 ion channel on erastin-induced chondrocytes, we first performed calcium imaging to detect  $Ca^{2+}$  influx. Consistent with previous reports [25], a robust  $Ca^{2+}$  influx was induced by naltriben, a known TRPM7 channel activator. Likewise, erastin exhibited a similar effect on the flow of calcium ions, which was abolished by pretreatment with 2-APB (Fig. 3E and F). Dysregulated  $Ca^{2+}$  influx is required for ferroptosis induced by GSH depletion [26]. To examine whether the effect of ferroptosis on chondrocytes is associated with intracellular  $Ca^{2+}$ , ethylene glycol tetraacetic acid (EGTA), a specific calcium chelator, was shown to restore chondrocyte viability and reduce cytotoxicity in erastin-induced chondrocytes (Fig. 3G, Figs. S4C and D). EGTA also relieved erastin-induced oxidative stress damage to chondrocytes as indicated by increased GSH levels, restore mitochondrial  $\Delta\Psi_m$  and decreased lipid ROS (Fig. 3H–J, Figs. S4D and E). Additionally, EGTA also reversed the erastin-induced increased ACSL4, NOX4 and decreased FTH and GPX4, suggesting that EGTA rescued erastin-induced ferroptosis in chondrocytes via chelating calcium (Fig. 3K). To determine the effect of TRPM7 kinase on chondrocyte ferroptosis, TG100-115, a potent TRPM7 kinase inhibitor, was evaluated. At low concentrations, only the kinase was inhibited, while at high TG100-115 concentrations both TRPM7 kinase and channel activity were inhibited [27]. Our results demonstrated high concentrations of TG100-115 could rescue chondrocytes ferroptosis, but not low-concentrations (Fig. 3L, Fig. S4F), indicating that indicating that it works through TRPM7 channel rather than kinase activity. Taken together, TRPM7 positively regulates chondrocyte ferroptosis through its channel activity *in vitro*.

### 3.4. PKC $\alpha$ is involved in TRPM7-mediated articular chondrocyte ferroptosis

To further explore the molecular basis for TRPM7-mediated chondrocyte ferroptosis, we performed RNA-sequencing (Fig. 4A). Principal component analysis (PCA) discriminated the gene expression distribution in the control group, erastin group and erastin+2-APB group (Fig. 4B). Moreover, we analyzed the differentially expressed genes (DEGs) among the three groups, and examined whether these genes were upregulated or downregulated after erastin stimulation and were reversed in the erastin+2-APB group. A total of 909 genes with logFc (Erastin+2-APB vs. Erastin)/logFc (Erastin vs. control) ratios not greater than 2 in absolute value were considered to be significantly reversed by 2-APB (Fig. 4C). Among these DEGs, enrichment analysis demonstrated inflammatory response-related pathways, RA-related processes and ferroptosis pathways to be enriched (Fig. 4D, Figs. S5A and B). Similarly, GSEA and heatmap analysis also showed that ferroptosis and RA-related gene expression signatures were highlighted between the indicated groups (Fig. 4E, Figs. S5C and D), suggesting that RA-related processes were associated with TRPM7-mediated chondrocyte ferroptosis induced by erastin.

Recent studies have demonstrated the calcium-activated Protein kinase C  $\alpha$  (PKC $\alpha$ ) signaling pathway to be involved in RA and ferroptosis [28,29]. Interestingly, RNA-sequencing results also revealed the PKC pathway triggered by erastin was regulated by 2-APB, which demonstrated that PKC may be associated with TRPM7-mediated chondrocyte ferroptosis (Fig. 4D). Further results displayed that the levels of p-PKC $\alpha$  were upregulated in both primary RACs and C28/I2 cells after erastin treatment, which could be abolished by PKC inhibitor bisindolylmaleimide I (BIM-I), TRPM7 channel inhibitor 2-APB or calcium chelator EGTA (Fig. 4F, Figs. S6A and B). Consistent with the above findings, TRPM7 knockdown also suppressed erastin-induced PKC $\alpha$  activation in C28/I2 cells (Fig. 4G). Collectively, these data imply that the activity of PKC $\alpha$  is regulated by TRPM7 in chondrocytes. Next, we investigated whether PKC $\alpha$  inhibition could reverse ferroptosis in chondrocytes. As expected, inhibition of PKC $\alpha$  with BIM-I rescued erastin-induced cell death, as shown as increased cell viability, restored  $\Delta\Psi_m$ , GSH, and reduced cytotoxicity, MDA and ROS production (Fig. 4H–K, Figs. S6C–E). Further, ACSL4 was elevated and SLC7A11, GPX4 were decreased in erastin-treated RACs and C28/I2 cells, which could be reversed by co-treatment of BIM-I (Fig. 4L, M, Fig. S6F). These results suggest that the PKC $\alpha$  pathway might be involved in TRPM7-mediated chondrocyte ferroptosis.

### 3.5. The interaction of PKC $\alpha$ with NOX4 participates in TRPM7-mediated articular chondrocyte ferroptosis

NOX4 is an important downstream PKC $\alpha$  effector molecule that plays a key role in the regulation of intracellular ROS production and oxidative stress [30,31]. NOX4 and its derived ROS can be induced by levels of calcium through PKC activation [32]. We speculated NOX4 expression to be regulated by the PKC pathway in ferroptotic chondrocytes. As expected, NOX4 was dramatically elevated in erastin-induced chondrocytes and significantly reduced by PKC $\alpha$  inhibition, suggesting that PKC $\alpha$  regulates NOX4 expression in ferroptotic chondrocytes (Fig. 5A and B). NOX activation is often modulated through protein-protein interaction and PKC $\alpha$  appears to have a major role in NOX activation through cytosolic subunit interactions [33]. To determine whether PKC $\alpha$  colocalizes with NOX4 in RACs, we performed Co-IP and immunofluorescence assays. Notably, immunofluorescence staining revealed an increased colocalization of PKC $\alpha$  and NOX4 in erastin-induced RACs, which was reduced by pretreatment with 2-APB (Fig. 5C and D). As shown in Fig. 5E and F, an interaction between PKC $\alpha$  and NOX4 was observed in primary RACs and C28/I2 cells.

To explore the binding sites between the two proteins, we constructed a model of the proposed PKC $\alpha$ : NOX4 heterodimer by molecular

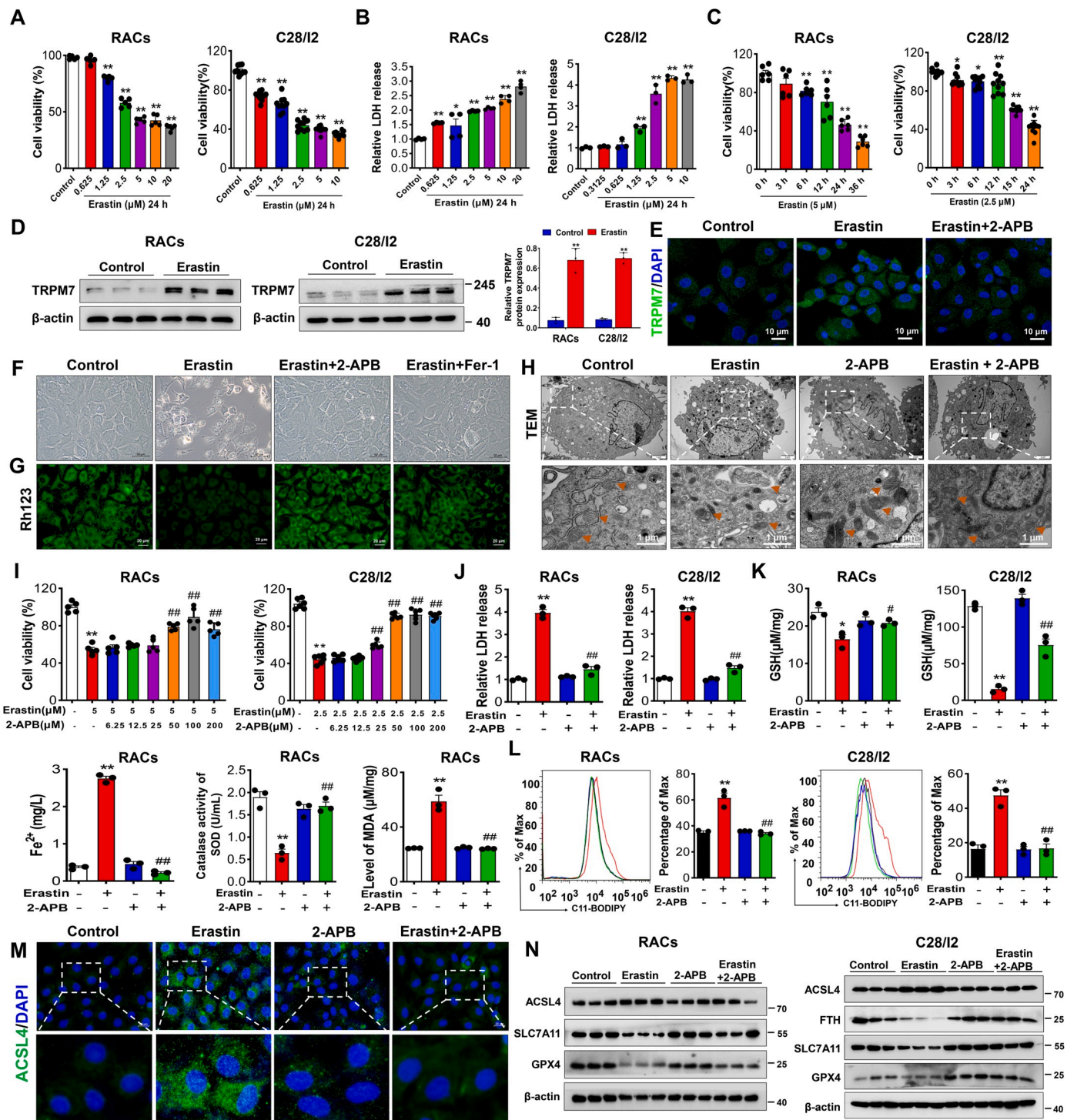


**Fig. 2.** Pharmacological blockade of TRPM7 protects against ferroptosis in primary rat articular chondrocytes (RACs) and C28/I2 cells. (A) Cell viability of RACs and C28/I2 cells treated with different concentrations of erastin for 24 h (n = 5–10). (B) LDH release of RACs and C28/I2 cells treated with different concentrations of erastin for 24 h (n = 3–4). (C) Cell viability of RACs and C28/I2 cells treated with erastin as indicated time (n = 6–10). (D) Western blot analysis for TRPM7 expression in RACs and C28/I2 cells treated with erastin for 24 h (n = 3). (E) Immunofluorescence for TRPM7 via using laser scanning confocal microscopy in RACs treated with/without erastin and 2-APB (100 μM) (n = 3). (F) Visualization of chondrocytes treated with/without erastin and 2-APB or Fer-1 (1 μM). (G) Measurement of ΔΨm by Rh123 in RACs in different treatment groups. (H) TEM of RACs treated with/without erastin and 2-APB. Orange triangles indicate mitochondria. (I) Cell viability of RACs and C28/I2 cells treated with erastin for 24 h in the presence of the different concentrations of 2-APB (n = 5–6). (J) LDH release of RACs and C28/I2 cells treated with/without erastin and 2-APB (n = 3). (K) LDH release, GSH, Fe<sup>2+</sup>, SOD and MDA were measured in RACs and C28/I2 cells treated with/without erastin and 2-APB (n = 3). (L) Lipid ROS production was assessed by C11-BODIPY in RACs and C28/I2 (n = 3). (M) Immunofluorescence staining for ACSL4 in RACs. (N) Western blot analysis for ferroptosis biomarkers ACSL4, SLC7A11, FTH and GPX4 in RACs and C28/I2 (n = 3). Data are means ± SD. \*P < 0.05, \*\*P < 0.01 erastin versus control; #P < 0.05, ##P < 0.01 erastin + 2-APB versus erastin. (For interpretation of the references to colour in this figure legend, the reader is referred to the Web version of this article.)

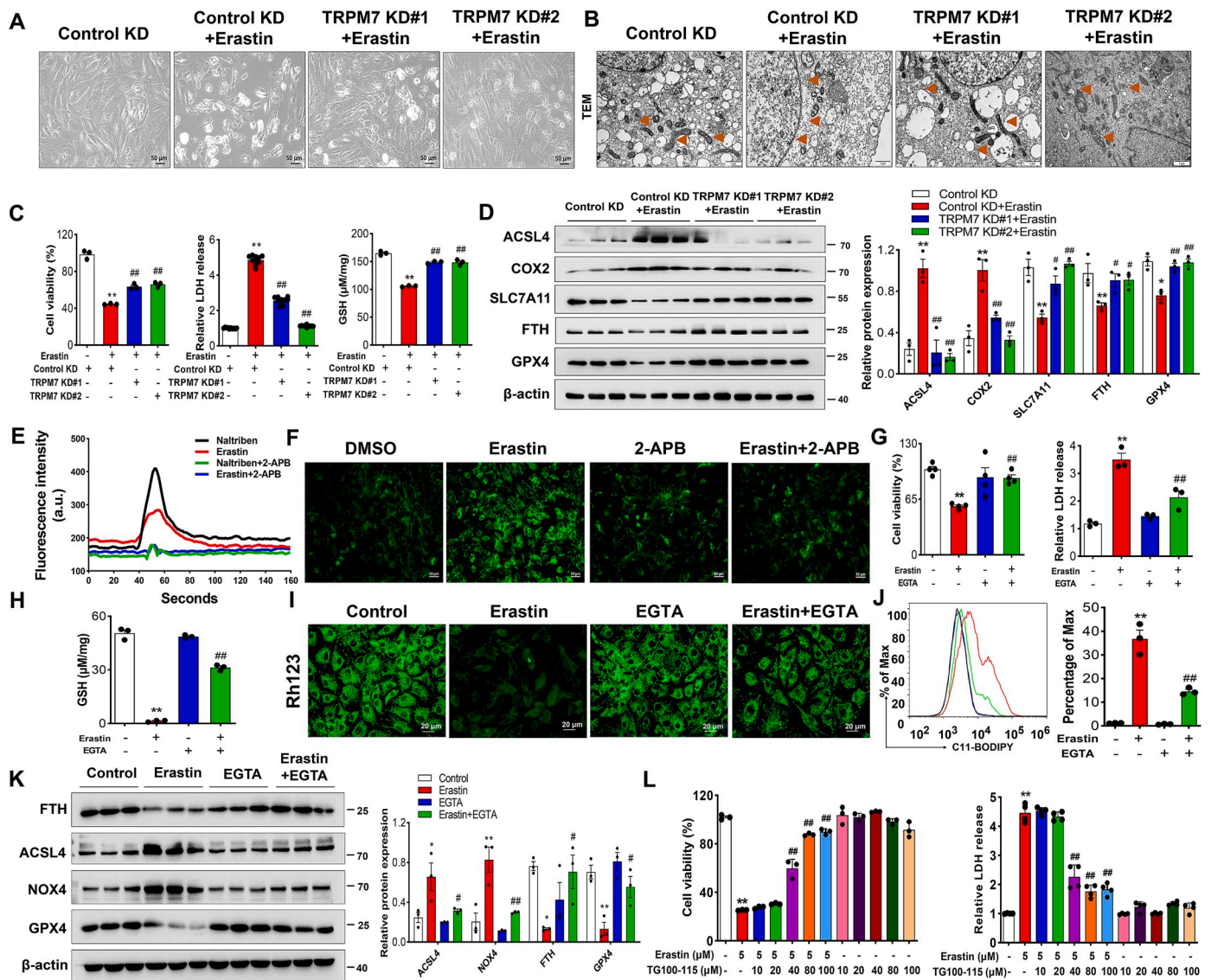
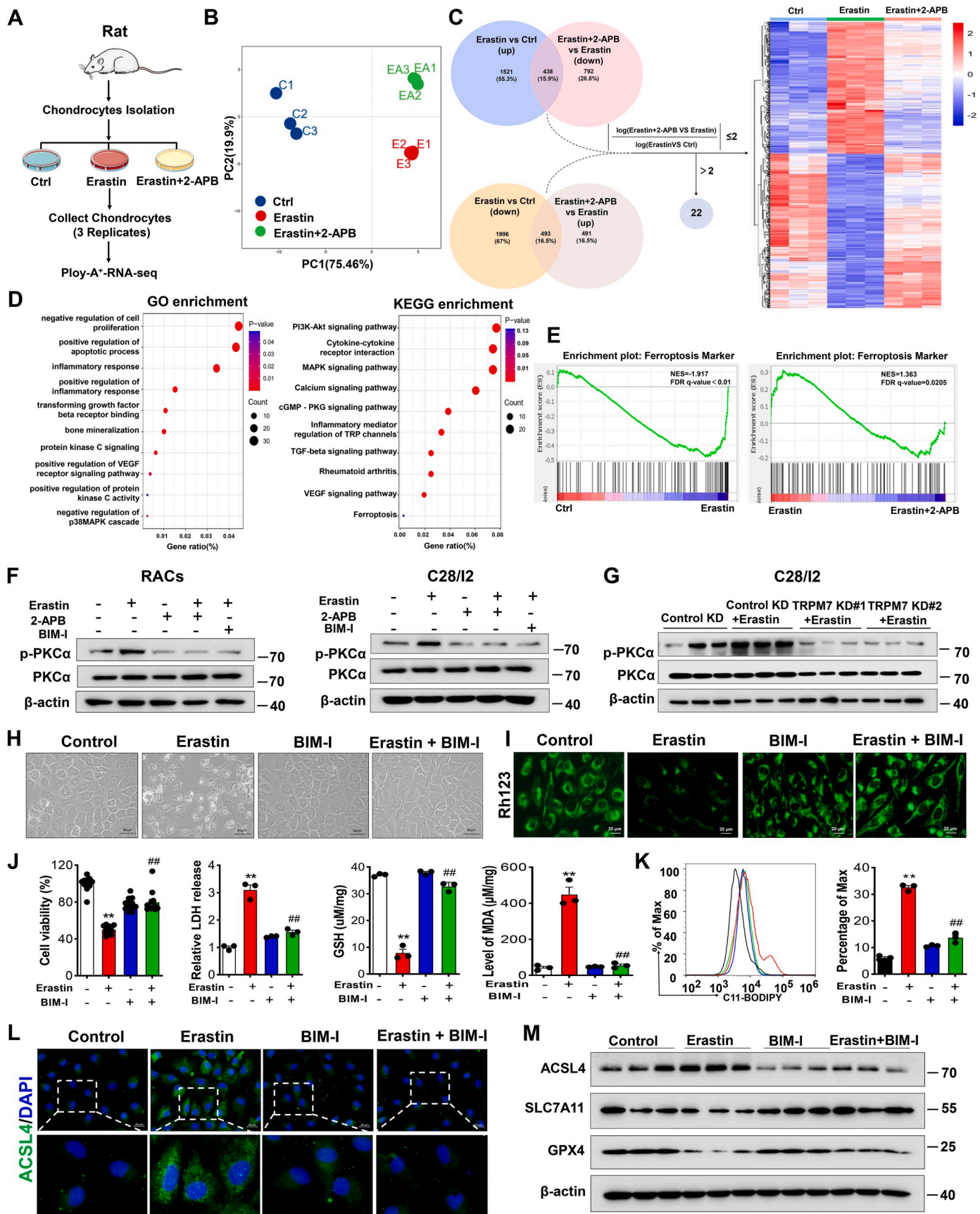


**Fig. 3.** Blockade of TRPM7 ion channel function protected against chondrocyte ferroptosis through a  $\text{Ca}^{2+}$ -dependent mechanism. (A, B) Visualization and TEM of indicated TRPM7 KD C28/I2 cells treated with erastin ( $2.5 \mu\text{M}$ , 12 h). Orange triangles indicate mitochondria. (C) Cell viability, LDH release and GSH in indicated TRPM7 KD C28/I2 cells ( $n = 3-10$ ). (D) Western blot analysis for ACSL4, COX2, SLC7A11, FTH and GPX4 in indicated TRPM7 KD C28/I2 cells ( $n = 3$ ). Data are means  $\pm$  SD.  $*P < 0.05$ ,  $**P < 0.01$ , Control KD + erastin versus Control KD;  $\#P < 0.05$ ,  $\#\#P < 0.01$ , TRPM7 KD + erastin versus Control KD + erastin. (E) Representative original traces of  $\text{Ca}^{2+}$  influx mediated by TRPM7 channels in RACs using Fluo-4 AM  $\text{Ca}^{2+}$  imaging. (F)  $\text{Ca}^{2+}$  dynamics were monitored using Fluo-4 AM in RACs following exposure to erastin ( $5 \mu\text{M}$ ) and 2-APB ( $100 \mu\text{M}$ ). (G, H) Cell viability, LDH release and GSH of RACs treated with/without erastin and EGTA ( $2 \text{ mM}$ ) ( $n = 3-4$ ). (I) Measurement of  $\Delta\Psi\text{m}$  by Rh123 in RACs in different treatment groups. (J) Lipid ROS production was assessed by C11-BODIPY in RACs ( $n = 3$ ). (K) Western blot analysis for ACSL4, NOX4, FTH and GPX4 in RACs ( $n = 3$ ). Data are means  $\pm$  SD.  $*P < 0.05$ ,  $**P < 0.01$  erastin versus control;  $\#P < 0.05$ ,  $\#\#P < 0.01$  erastin + EGTA versus erastin. (L) Cell viability and LDH release of RACs treated with/without erastin and different concentrations of TG100-115 for 24 h ( $n = 3-4$ ). Data are means  $\pm$  SD.  $**P < 0.01$  erastin versus control;  $\#\#P < 0.01$  erastin + TG100-115 versus erastin. (For interpretation of the references to colour in this figure legend, the reader is referred to the Web version of this article.)

docking analysis, which showed that NOX4 and PKC $\alpha$  proteins had three binding regions, among which NOX4 had 45 amino acid residues, and PKC $\alpha$  protein had 33 amino acid residues within the binding regions (Fig. 5G). Root mean square deviation (RMSD) results showed that the protein structure of the complex was relatively stable for 20–40 ns (Fig. S7). Per-residue energy decomposition and alanine scanning results found that the NOX4 residue (R231) contributed the most to the stability of the complex, interacting by hydrogen-bonding with PKC $\alpha$  residues (G7 and T11) (Fig. 5H–J). Collectively, these results suggest that TRPM7 might regulate PKC $\alpha$ -NOX4 interaction in chondrocyte ferroptosis.

### 3.6. NOX4 contributes to TRPM7-mediated ferroptosis of primary rat articular chondrocytes and C28/I2 cells

Intracellular NOX4-mediated ROS and oxidative stress are known to be closely related to ferroptosis [34]. To explore NOX4 involvement in TRPM7-regulated chondrocyte ferroptosis, an inhibitor of NOX4, GKT137831, was assessed. Our results showed that the increase of NOX4 could be reversed by TRPM7 suppression or knockdown in erastin-induced RACs and C28/I2 cells (Fig. 6A–C), suggesting NOX4 is an effector of TRPM7 activation. Furthermore, inhibition of NOX4 suppressed chondrocyte ferroptosis, showing increased cell viability, reduced cytotoxicity, ROS production and iron overload and restoration of redox balance (Fig. 6D–I, Figs. S8A and B). Increased expression of



(caption on next page)

**Fig. 4.** Blockade of PKC $\alpha$  protects against ferroptosis in primary rat articular chondrocytes. (A) Schematic diagram of RNA sequencing design and sample preparation procedures. (B) Principal component analysis (PCA) discriminating the gene expression distribution among the control, erastin and erastin +2-APB groups. (C) Venn diagram showing these overlapping genes between two clusters (erastin versus control and erastin +2-APB versus erastin) to obtain heatmap of DEGs. (D) GO and KEGG enrichment analyses showing biological processes and signaling pathways associated with these DEGs, respectively. (E) GSEA showing ferroptosis processes and pathways in the erastin versus control group or erastin +2-APB versus erastin group (n = 3). (F) Western blot analysis for p-PKC $\alpha$  and PKC $\alpha$  in erastin-induced RACs and C28/I2 cells treated with/without BIM-I (5  $\mu$ M) or 2-APB (100  $\mu$ M). (G) Western blot analysis for p-PKC $\alpha$  and PKC $\alpha$  in indicated TRPM7 KD C28/I2 cells (n = 3). (H) Visualization of RACs treated with/without erastin and BIM-I. (I) Measurement of  $\Delta\Psi_m$  by Rh123 in RACs. (J) Cell viability, LDH release, GSH and MDA of RACs and C28/I2 cells (n = 3–12). (K) Lipid ROS production was assessed by flow cytometry using C11-BODIPY in RACs (n = 3). (L) Immunofluorescence staining for ACSL4 in RACs. (M) Western blot analysis for ACSL4, SLC7A11 and GPX4 in RACs (n = 3). Data are means  $\pm$  SD. \*\**P* < 0.01 erastin versus control; ##*P* < 0.01 erastin + BIM-I versus erastin.

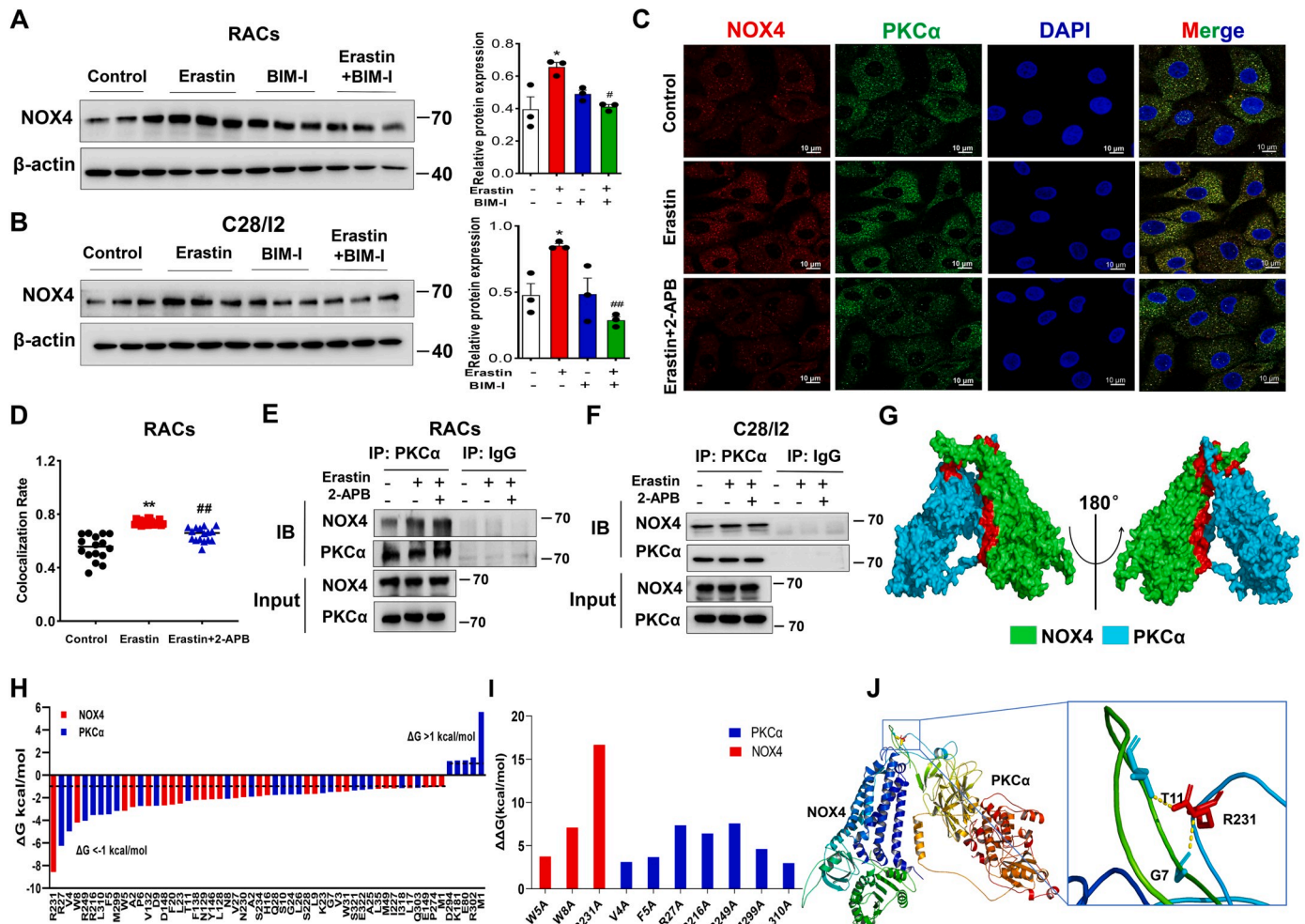


**Fig. 5.** Blockade of TRPM7 suppresses PKC $\alpha$ -NOX4 interaction in articular chondrocytes. (A, B) Western blot analysis for NOX4 in erastin-induced RACs and C28/I2 cells treated with BIM-I (n = 3). Data are means  $\pm$  SD. \**P* < 0.05, erastin versus control; #*P* < 0.05, ##*P* < 0.01 erastin + BIM-I versus erastin. (C) Representative photomicrographs of RACs stained to detect NOX4 (red fluorescence), PKC $\alpha$  (green fluorescence), and the nucleus (DAPI, blue fluorescence) treated with/without erastin (5  $\mu$ M) and 2-APB (100  $\mu$ M). (D) Colocalization rate of NOX4/PKC $\alpha$  in erastin-induced RACs treated with/without 2-APB (n = 16). Data are means  $\pm$  SD. \*\**P* < 0.01 erastin versus control; ##*P* < 0.01 erastin + 2-APB versus erastin. (E, F) The interaction between PKC $\alpha$  and NOX4 in primary RACs and C28/I2 cells was analyzed by co-immunoprecipitation. (G) 3D binding structure of PKC $\alpha$  and NOX4 determined via molecular modeling and docking studies. (H) The energy values of NOX4 residues (R231, W8, W5) and PKC $\alpha$  residues (R27, V4, R249, R216, L310, F5, M299) were less than  $-3$  kcal/mol by per-residue energy decomposition analysis. Dashed lines indicate thresholds less than  $-1$  or greater than  $1$  kcal/mol. (I) Alanine scanning results showed the contributions of protein residues to the stability of the NOX4/PKC $\alpha$  complex. (J) Close-up view of hydrogen bonding between NOX4 residue R231 and PKC $\alpha$  residues (G7 and T11). (For interpretation of the references to colour in this figure legend, the reader is referred to the Web version of this article.)

ACSL4 and NOX4, as well as decreased expression of SLC7A11, FTH, and GPX4 induced by erastin were reversed by blockade of NOX4 (Fig. 6J, Fig. S8C), suggesting that pharmacological inhibition of NOX4 prevents chondrocyte ferroptosis. To further confirm the role of NOX4 in TRPM7-mediated chondrocyte ferroptosis, NOX4 was overexpressed in TRPM7 knockdown C28/I2 cells. Interestingly, upregulation of NOX4 abolished the protective effects of TRPM7 knockdown on erastin-induced ferroptosis, accompanied by decreased cell viability,

GSH and increased cytotoxicity (Fig. 6K). Furthermore, NOX4 overexpression reversed the decreased ACSL4 and the increased SLC7A11 and GPX4 caused by TRPM7 knockdown in erastin-induced C28/I2 cells (Fig. 6L). Taken together, these results reveal that NOX4 as the TRPM7 downstream molecule plays a critical role in promoting chondrocyte ferroptosis.

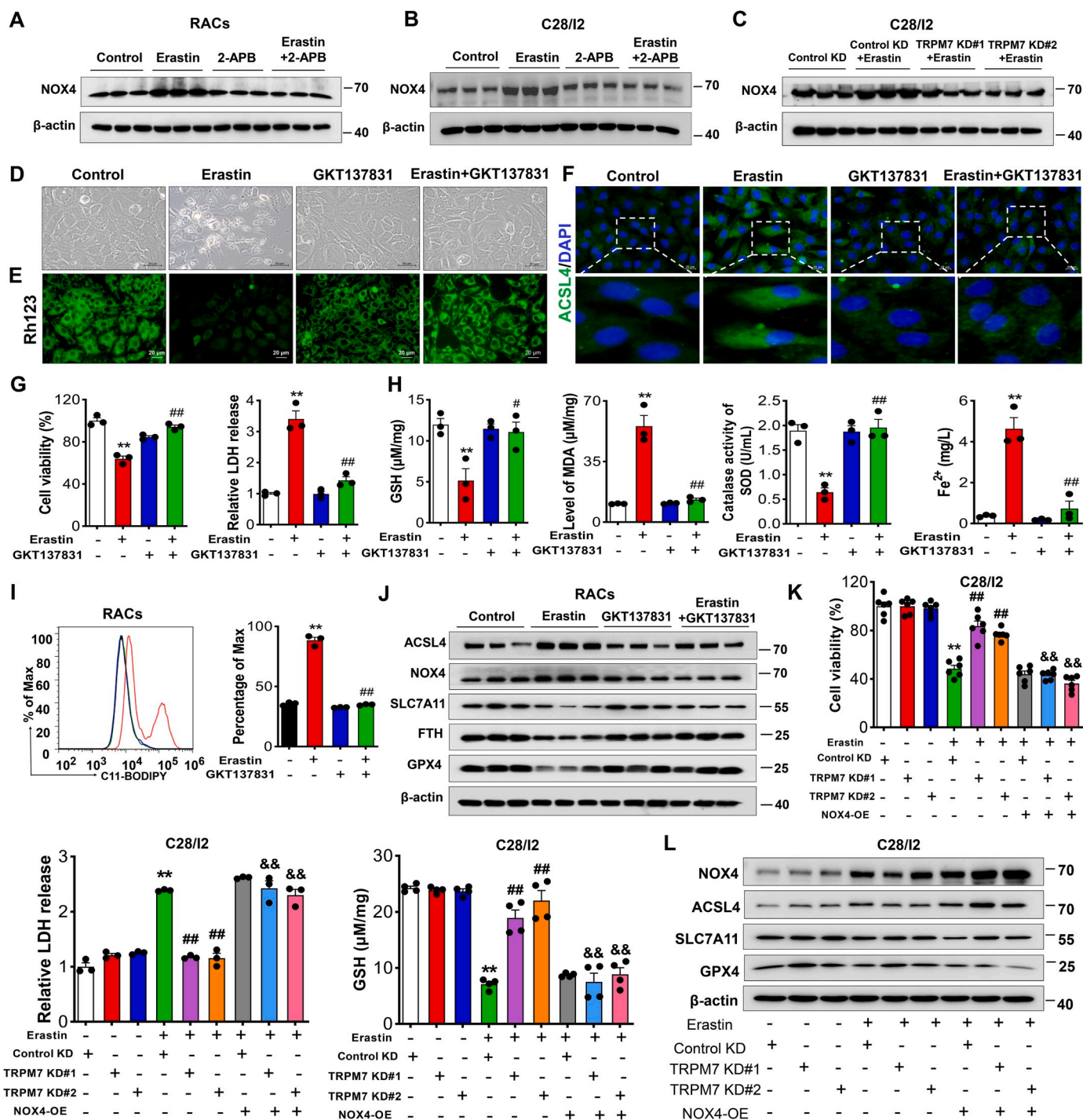


**Fig. 6.** NOX4 promotes TRPM7-mediated ferroptosis in primary rat articular chondrocytes and C28/I2 cells. (A, B) Western blot analysis for NOX4 in erastin-induced RACs and C28/I2 cells treated with/without 2-APB (100  $\mu$ M). Data are means  $\pm$  SD, n = 3. (C) Western blot analysis for NOX4 in indicated TRPM7 KD C28/I2 cells treated with erastin (2.5  $\mu$ M, 12 h). Data are means  $\pm$  SD, n = 3. (D) Visualization of RACs cell viability treated with/without erastin (5  $\mu$ M) and GKT137831 (20  $\mu$ M). (E) Measurement of  $\Delta\Psi_m$  in RACs. (F) Immunofluorescence staining for ACSL4 in RACs. (G) Cell viability and LDH release of RACs (n = 3). (H) GSH,  $Fe^{2+}$ , SOD and MDA were measured in RACs (n = 3). (I) Lipid ROS production was assessed by flow cytometry using C11-BODIPY in RACs (n = 3). Data are means  $\pm$  SD. **\*\****P* < 0.01 erastin versus control; **#***P* < 0.05, **##***P* < 0.01 erastin + GKT137831 versus erastin. (J) Western blot analysis for ACSL4, NOX4, SLC7A11, FTH and GPX4 in RACs (n = 3). (K) Cell viability, LDH release and GSH of erastin-induced TRPM7 KD C28/I2 cells with NOX4 OE (n = 3–6). (L) Western blot analysis for ACSL4, SLC7A11, NOX4 and GPX4 in erastin-induced TRPM7 KD C28/I2 cells with NOX4 overexpression (n = 3). Data are means  $\pm$  SD. **\*\****P* < 0.01 Control KD + erastin versus Control KD; **##***P* < 0.01 TRPM7 KD + erastin versus Control KD + erastin, **&&***P* < 0.01 TRPM7 KD + NOX4 OE + erastin versus TRPM7 KD + erastin.

**3.7. TRPM7 deficiency negatively regulates CFA-induced AA rat pathogenic signatures and chondrocyte ferroptosis**

To clarify the contribution of TRPM7 to RA disease onset or

progression, we established TRPM7 knockdown rats by intra-articular injection of AAV9 expressing TRPM7-specific shRNA (Fig. 7A). The efficiency of AAV9 expressing TRPM7-specific shRNA in rat joints was verified by *in vivo* small animal imaging and immunofluorescence

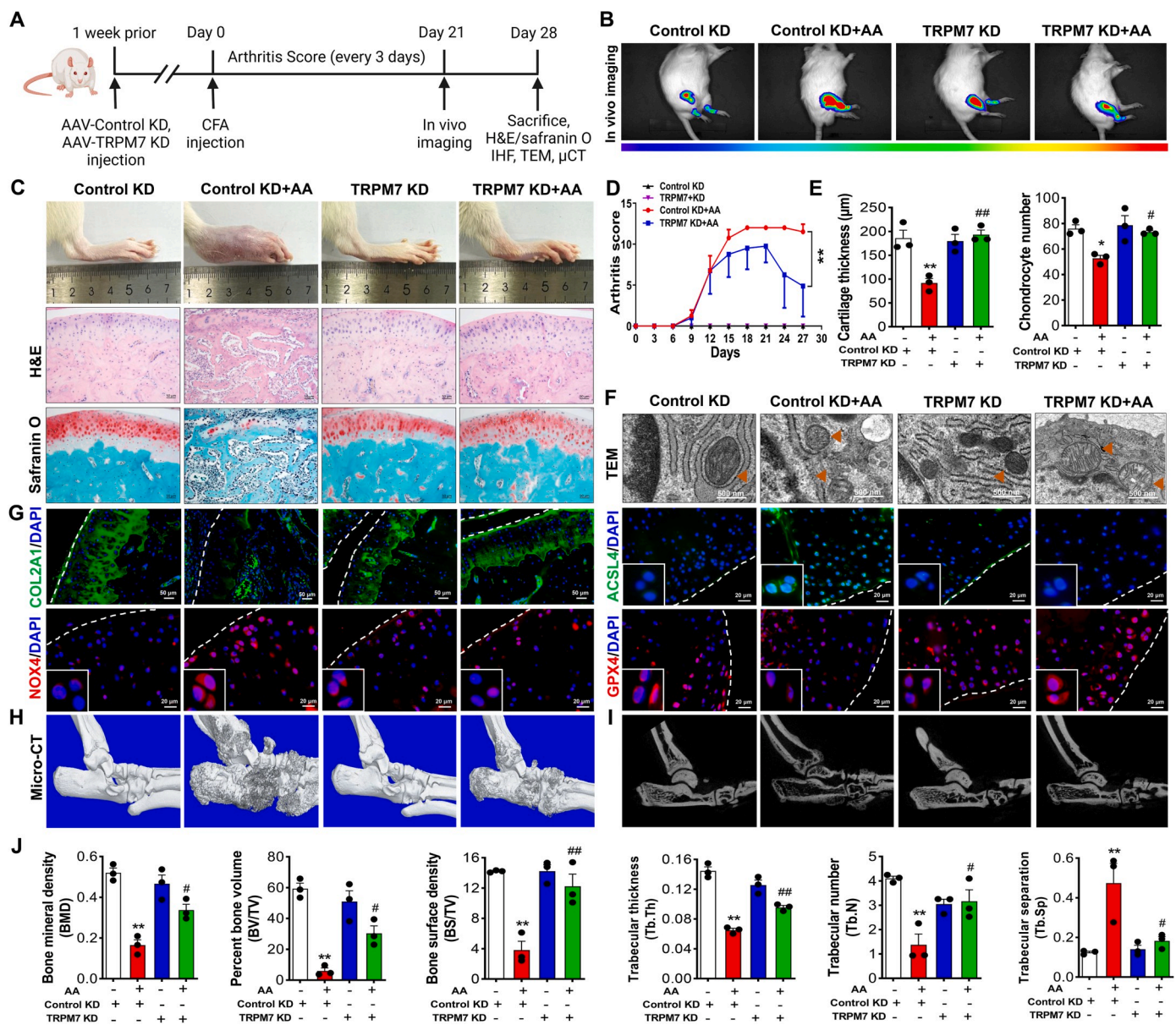


**Fig. 7.** TRPM7 knockdown attenuated CFA-induced rat AA development and protected cartilage destruction and bone erosion by suppressing ferroptosis. (A) Timeline of animal experiment. (B) Representative IVIS images depicting D-luciferin biodistribution in normal and AA rats treated with AAV9 expressing negative control shRNA or with TRPM7 specific shRNA ( $n = 3$  rats). (C) Representative of ankle joints image, H&E staining and safranin O/fast green staining on cartilages. (D) Arthritis swelling severity scores in AA rats ( $n = 8$  rats). (E) Articular cartilage thickness and chondrocyte number in AA rats ( $n = 3$  rats). (F) Representative TEM images of rats in indicated groups ( $n = 3$  rats). Orange triangles indicate mitochondria. (G) Immunostaining of COL2A1, ACSL4, NOX4 and GPX4 in cartilages. White dashed lines indicate the cartilage margin. (H) Micro-CT analysis for the ankles of rats in indicated groups. (I) Representative micro-CT images of the trabecular in bone. (J) Quantitative analysis of bone mineral density (BMD), bone volume to tissue volume (BV/TV), bone surface to tissue volume (BS/TV), trabecular thickness (Tb.Th), trabecular number (Tb.N) and trabecular separation (Tb.Sp) were measured ( $n = 3$  rats). Data are means  $\pm$  SEM. \* $P < 0.05$ , \*\* $P < 0.01$  Control KD + AA versus Control KD; # $P < 0.05$ , ## $P < 0.01$  TRPM7 KD + AA versus Control KD + AA. (For interpretation of the references to colour in this figure legend, the reader is referred to the Web version of this article.)

(Fig. 7B, Fig. S9A). Histopathologic evaluation showed TRPM7 knockdown or pharmacological blockade to alleviate AA rat cartilage damage and restore cartilage thickness and collagen levels (Fig. 7C, Figs. S10A–E). Arthritis swelling severity scores and the loss of articular cartilage thickness and chondrocyte number in per defined cartilage area were reversed by TRPM7 knockdown (Fig. 7D and E). Chondrocytes embedded in AA cartilages demonstrated shrunken mitochondria with increased membrane density as well as rupture of outer mitochondrial membrane, while knockdown and pharmacological blockade of TRPM7 obviously protected morphological and ultrastructural alterations of the mitochondria in the AA rat chondrocytes (Fig. 7F, Fig. S11A).

Remarkably, immunostaining also indicated the reduced ACSL4, p-PKC $\alpha$ , NOX4 and increased COL2A1, GPX4 expression after down-regulation of TRPM7 in cartilages (Fig. 7G, Fig. S9B, Fig. S10E, Fig. S11B, Figs. S12A–D). Interestingly, AA rats treated with ferroptosis inhibitor liproxstatin-1 had similar protective effects on cartilages *in vivo* through the suppression of chondrocyte ferroptosis (Figs. S12A–D). Micro-CT scan displayed apparent cartilage destruction, rough bone surfaces and bone erosion in AA rats. In contrast, TRPM7 knockdown effectively alleviated the cartilage and bone destruction in AA rats (Fig. 7H–J). Taken together, TRPM7 plays a crucial role in AA pathogenesis and chondrocyte ferroptosis through suppression of the PKC $\alpha$ -NOX4 axis.

#### 4. Discussion

Destruction of articular cartilage and bone tissue results in RA patient disability, and the death of articular chondrocytes is the main initiating factor of cartilage destruction. Therefore, the development of a targeted inhibition of RA articular chondrocyte death would significantly contribute to the prevention and treatment of RA. Ferroptosis is a new programmed death mode that plays a key role in a variety of pathological and physiological processes and is closely related to human disease progression, including the pathogenesis of arthritis. However, it is still unclear whether ferroptosis occurs in RA articular chondrocytes and whether it plays a role in the destruction of articular cartilage. In this study, we first found significant ferroptosis in articular chondrocytes of RA patients and AA rats, and demonstrated inhibition of chondrocyte ferroptosis to protect articular cartilage from damage in AA rats. Further, we found abnormally high levels of TRPM7 in the articular cartilage of RA patients and AA rats, as well as TRPM7 regulation of chondrocyte ferroptosis. Mechanistically, both genetic and pharmacological inhibition of TRPM7 attenuated articular chondrocyte ferroptosis and cartilage destruction via the PKC $\alpha$ -NOX4 axis (Fig. 8), suggesting that TRPM7-mediated ferroptosis in chondrocytes is a promising target for the prevention and treatment of RA.

The pathogenesis of RA is very complex, involving immune cell populations, inflammatory factors, and oxidative stress [35]. Recent interest has focused upon the role of articular chondrocyte death in disease pathogenesis and upon the observation that cartilage is not a passive tissue damaged by synovial inflammation. Primary cartilage damage appears to constitute a prerequisite for RA joint pathogenesis, with cartilage damage often preceding synovial invasion [36]. RA chondrocytes can be targeted by inflammatory mediators and by effector cells, resulting in direct or indirect articular cartilage damage. Studies have found that ferroptosis exists in articular chondrocytes in osteoarthritis, and intra-articular injection of Fer-1, and iron chelator deferoxamine could significantly inhibit ferroptosis of chondrocytes and attenuate the progression of osteoarthritis [37,38]. Previously, serum ROS and lipid peroxidation levels were found to be significantly increased in RA patients, which is consistent with characteristics of ferroptosis [39]. Recent studies have confirmed that RA synoviocytes undergo ferroptosis, and administration of ferroptosis inducers can further induce ferroptosis in synoviocytes and alleviate RA symptoms [13]. Ling et al. found that ferroptosis of RA synoviocytes was

significantly reduced compared to normal synoviocytes, and that erastin treatment induced synoviocyte ferroptosis, reducing synovial hyperplasia [11]. In this study, we found that compared with the normal group, abundant ferroptosis occurred in articular chondrocytes of RA patients and AA rats, and that inhibition of chondrocyte ferroptosis protected from articular cartilage damage in AA rats. These results demonstrate that ferroptosis exists in RA articular chondrocytes. Given that both synoviocytes and chondrocytes undergo ferroptosis during the pathogenesis of RA, cell-specific targeted treatments are necessary to reduce the side effects of RA treatments that target ferroptosis.

TRPM7, a transmembrane protein with dual functions of cation channel and kinase activity, plays an important role in various pathophysiological processes such as cell proliferation, death, and inflammation by regulating ion influx and signal transduction [40]. Oxidative stress accompanying pathological reactions activates TRPM7, mediates the influx of Ca<sup>2+</sup> and participate in the progression of various diseases [41,42]. TRPM7 activation leads to neuron death via mediating Ca<sup>2+</sup> overload and ROS production, with suppression of TRPM7 significantly reducing oxidative damage [43,44]. Further, the channel-kinase of TRPM7 is functionally expressed in neutrophils, playing an essential role in neutrophil recruitment during inflammation [45]. Our previous study found that blockade of TRPM7 had a protective effect on RA articular cartilage destruction [20]. Herein, results displayed that both genetic and pharmacological inhibition of TRPM7 significantly inhibited erastin-induced chondrocyte ferroptosis and AA articular cartilage and bone destruction. Moreover, chondrocyte ferroptosis was inhibited by blockade of TRPM7-mediated elevation of intracellular Ca<sup>2+</sup>, while inhibition of TRPM7 kinase activity had no effects, suggesting that TRPM7 channel activity plays a key regulatory role in RA articular chondrocyte ferroptosis.

Oxidative stress results from an imbalance in production and scavenging of free radicals, with excess ROS/RNS producing oxidative damage of tissues and cells. Oxidative stress and the accumulation of lipid peroxidation are important drivers of chronic inflammation in joints [13]. Therefore, modulation of oxidative microenvironment is considered a promising strategy for treatment of RA. Ferroptosis is a regulated form of cell death characterized by increased intracellular ROS levels and lipid peroxidation [46]. NADPH oxidase (NOX) is a multi-subunit complex, a key enzyme in redox signaling, and one of the primary sources of ROS. Calcium ions and their activated protein kinases can activate NOX through a protein phosphorylation mechanism. It has

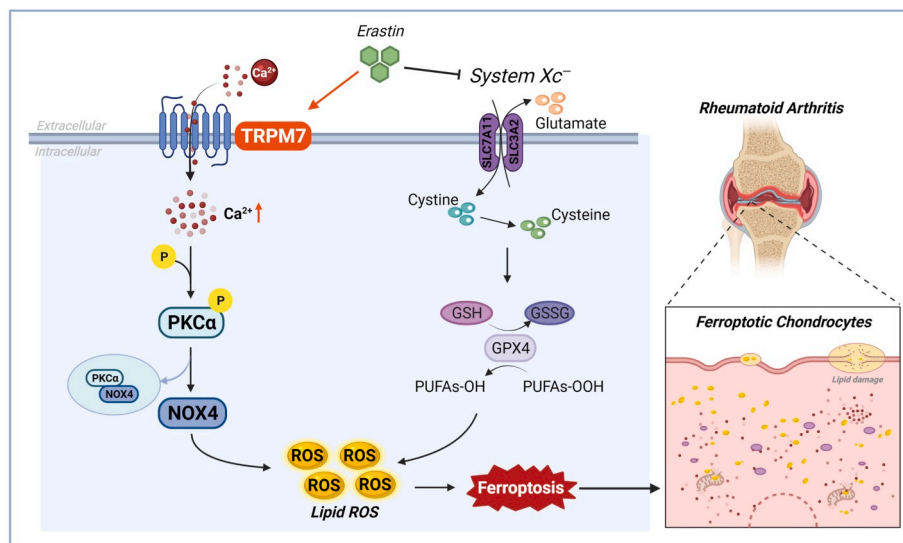


**Fig. 8.** TRPM7 channel mediate ferroptosis in RA chondrocytes through regulating PKC $\alpha$ -NOX4 axis. System Xc<sup>-</sup> inhibition and GSH depletion-mediated TRPM7 upregulation triggers PKC $\alpha$  activation via direct binding with NOX4 domain, thus aggravating the accumulation of ROS and lipid peroxidation, and eventually leading to ferroptosis in RA chondrocytes (Created with BioRender.com).

been reported that blocking TRPM7 can reduce PKC-dependent NOX activity by inhibiting  $\text{Ca}^{2+}$  influx, thereby inhibiting LPS-induced ROS production [47]. Interestingly, genetic and pharmacological inhibition of PKC $\alpha$  significantly reduced erastin-induced ferroptosis [48]. Furthermore, the NOX1/4 isoform inhibition also significantly decreased erastin-stimulated ROS, lipid ROS and cell death [49]. Our results demonstrate that blockade of PKC $\alpha$  or NOX4 can inhibit lipid peroxidation and chondrocyte ferroptosis. Interestingly, blocking PKC $\alpha$  could significantly down-regulate NOX4 expression and the interaction of PKC $\alpha$  with NOX4. Furthermore, in silico molecular simulations and alanine scanning found that R231 of the NOX4 protein maximally contributed the stability of the NOX4: PKC $\alpha$  complex. Although probable key binding sites for PKC $\alpha$  and NOX4 were predicted, further investigations are needed to verify these findings. Of particular note, inhibition of TRPM7 reduced PKC $\alpha$  activation, NOX4 expression, and the interaction between PKC $\alpha$  and NOX4, suggesting that TRPM7 may regulate RA articular chondrocyte ferroptosis through the PKC $\alpha$ -NOX4 signaling pathway.

In conclusion, we demonstrated, for the first time, that TRPM7 was the main critical regulatory target in RA articular chondrocyte ferroptosis and RA progression. Meanwhile, we also identified 2-APB might be used as a potential potent ferroptosis inhibitor. TRPM7 deficiency reduced chondrocyte ferroptosis and led to inhibition of cartilage and bone destruction. Therefore, targeting TRPM7 may be potent therapeutic approaches for controlling RA articular cartilage and bone destruction.

#### Author contributions

R.P.Z., Y.C. and S.F.L performed most of the experiments, analyzed data and wrote the manuscript. X.W., W.J.H., Y.L., L.D., R.D.Z., Y.J.Z. and X.W.F. helped with cell culture. J.D., F.C. and H.L.Z. helped with collecting animal samples and data analysis. W.R.H. and W.J.F. analyzed RNA-seq data and in silico molecular modeling and docking. S. A.T., K.W., and F.H.C. revised the paper. W.H., C.H.D., and R.P.Z. designed the project and supervised the study. All authors agreed on the final version of the paper.

#### Declaration of competing interest

The authors declare no competing interests.

#### Data availability

Data will be made available on request.

#### Acknowledgements

This work was supported by grants from the National Natural Science Foundation of China (81902182, 82071591), the Natural Science Foundation Incubation Program of The Second Hospital of Anhui Medical University (2021GMFY06).

#### Appendix A. Supplementary data

Supplementary data to this article can be found online at <https://doi.org/10.1016/j.redox.2022.102411>.

#### References

- [1] C. Deng, et al., Targeted apoptosis of macrophages and osteoclasts in arthritic joints is effective against advanced inflammatory arthritis, *Nat. Commun.* 12 (2021) 2174.
- [2] P. Ren, H. Niu, H. Gong, R. Zhang, Y. Fan, Morphological, biochemical and mechanical properties of articular cartilage and subchondral bone in rat tibial plateau are age related, *J. Anat.* 232 (2018) 457–471.
- [3] M. Ostrowska, W. Maslinski, M. Prochoc-Sobieszek, M. Nieciecki, I. Sudol-Szopinska, Cartilage and bone damage in rheumatoid arthritis, *Reumatologia* 56 (2018) 111–120.
- [4] S. Park, I.J. Baek, J.H. Ryu, C.H. Chun, E.J. Jin, PPAR $\alpha$ -ACOT12 axis is responsible for maintaining cartilage homeostasis through modulating de novo lipogenesis, *Nat. Commun.* 13 (2022) 3.
- [5] M. Li, et al., The immune microenvironment in cartilage injury and repair, *Acta Biomater.* 140 (2022) 23–42.
- [6] T. Pap, A. Korb-Pap, Cartilage damage in osteoarthritis and rheumatoid arthritis—two unequal siblings, *Nat. Rev. Rheumatol.* 11 (2015) 606–615.
- [7] R.P. Zhou, et al., Novel insights into ferroptosis: implications for age-related diseases, *Theranostics* 10 (2020) 11976–11997.
- [8] C. Guo, L. Sun, X. Chen, D. Zhang, Oxidative stress, mitochondrial damage and neurodegenerative diseases, *Neural Regen Res* 8 (2013) 2003–2014.
- [9] S. Jang, et al., Elucidating the contribution of mitochondrial glutathione to ferroptosis in cardiomyocytes, *Redox Biol.* 45 (2021), 102021.
- [10] A. Wu, et al., Fibroblast growth factor 21 attenuates iron overload-induced liver injury and fibrosis by inhibiting ferroptosis, *Redox Biol.* 46 (2021), 102131.
- [11] H. Ling, et al., Glycine increased ferroptosis via SAM-mediated GPX4 promoter methylation in rheumatoid arthritis, *Rheumatology* (2022), <https://doi.org/10.1093/rheumatology/keac069>.
- [12] H. Luo, R. Zhang, Icarin enhances cell survival in lipopolysaccharide-induced synoviocytes by suppressing ferroptosis via the Xc-/GPX4 axis, *Exp. Ther. Med.* 21 (2021) 72.
- [13] J. Wu, et al., TNF antagonist sensitizes synovial fibroblasts to ferroptotic cell death in collagen-induced arthritis mouse models, *Nat. Commun.* 13 (2022) 676.
- [14] M. Li, et al., Molecular determinants of Mg $^{2+}$  and Ca $^{2+}$  permeability and pH sensitivity in TRPM6 and TRPM7, *J. Biol. Chem.* 282 (2007) 25817–25830.
- [15] D.E. Clapham, TRP channels as cellular sensors, *Nature* 426 (2003) 517–524.
- [16] L.V. Ryazanova, Z. Hu, S. Suzuki, V. Chubanov, A. Fleig, A.G. Ryazanov, Elucidating the role of the TRPM7 alpha-kinase: TRPM7 kinase inactivation leads to magnesium deprivation resistance phenotype in mice, *Sci. Rep.* 4 (2014) 7599.
- [17] T. Sonou, et al., Magnesium prevents phosphate-induced vascular calcification via TRPM7 and Pit-1 in an aortic tissue culture model, *Hypertens. Res.* 40 (2017) 562–567.
- [18] M. Aarts, et al., Treatment of ischemic brain damage by perturbing NMDA receptor-PSD-95 protein interactions, *Science* 298 (2002) 846–850.
- [19] S. Gatica, et al., TRPM7 mediates kidney injury, endothelial hyperpermeability and mortality during endotoxemia, *Lab. Invest.* 100 (2020) 234–249.
- [20] G. Ma, et al., Blockade of TRPM7 alleviates chondrocyte apoptosis and articular cartilage damage in the adjuvant arthritis rat model through regulation of the Indian hedgehog signaling pathway, *Front. Pharmacol.* 12 (2021), 655551.
- [21] R. Zhou, et al., ASIC2a overexpression enhances the protective effect of Pctx1 and APETx2 against acidosis-induced articular chondrocyte apoptosis and cytotoxicity, *Gene* 642 (2018) 230–240.
- [22] F. Sivandzade, A. Bhalerao, L. Cucullo, Analysis of the mitochondrial membrane potential using the cationic JC-1 dye as a sensitive fluorescent probe, *Bio Protoc* 9 (2019).
- [23] S. Gatica, F. Eltit, J.F. Santibanez, D. Varela, C. Cabello-Verrugio, F. Simon, Expression suppression and activity inhibition of TRPM7 regulate cytokine production and multiple organ dysfunction syndrome during endotoxemia: a new target for sepsis, *Curr. Mol. Med.* 19 (2019) 547–559.
- [24] V. Chubanov, et al., Natural and synthetic modulators of SK (K $_{Ca}$ ) $_{2}$  potassium channels inhibit magnesium-dependent activity of the kinase-coupled cation channel TRPM7, *Br. J. Pharmacol.* 166 (2012) 1357–1376.
- [25] G.H. Souza Bomfim, V. Costiniti, Y. Li, Y. Idaghdour, R.S. Lacruz, TRPM7 activation potentiates SOCE in enamel cells but requires ORAI, *Cell Calcium* 87 (2020), 102187.
- [26] N. Henke, et al., The plasma membrane channel ORAI1 mediates detrimental calcium influx caused by endogenous oxidative stress, *Cell Death Dis.* 4 (2013), e470.
- [27] C. Song, et al., Identification of TG100-115 as a new and potent TRPM7 kinase inhibitor, which suppresses breast cancer cell migration and invasion, *Biochim. Biophys. Acta Gen. Subj.* 1861 (2017) 947–957.
- [28] Q. Bai, et al., Protein kinase C- $\alpha$  upregulates sodium channel Nav1.9 in nociceptive dorsal root ganglion neurons in an inflammatory arthritis pain model of rat, *J. Cell. Biochem.* 121 (2020) 768–778.
- [29] L. Monteleone, et al., PKC $\alpha$  inhibition as a strategy to sensitize neuroblastoma stem cells to etoposide by stimulating ferroptosis, *Antioxidants* 10 (2021).
- [30] X.F. Wei, Q.G. Zhou, F.F. Hou, B.Y. Liu, M. Liang, Advanced oxidation protein products induce mesangial cell perturbation through PKC-dependent activation of NADPH oxidase, *Am. J. Physiol. Ren. Physiol.* 296 (2009) F427–F437.
- [31] H. Xu, et al., Differential roles of PKC $\alpha$  and PKC $\epsilon$  in controlling the gene expression of Nox4 in human endothelial cells, *Free Radic. Biol. Med.* 44 (2008) 1656–1667.
- [32] Y. Xun, et al., Role of Nox4 in high calcium-induced renal oxidative stress damage and crystal deposition, *Antioxidants Redox Signal.* 36 (2022) 15–38.
- [33] R. Rastogi, X. Geng, F. Li, Y. Ding, NOX activation by subunit interaction and underlying mechanisms in disease, *Front. Cell. Neurosci.* 10 (2016) 301.
- [34] M.W. Park, et al., NOX4 promotes ferroptosis of astrocytes by oxidative stress-induced lipid peroxidation via the impairment of mitochondrial metabolism in Alzheimer's diseases, *Redox Biol.* 41 (2021), 101947.
- [35] U. Fearon, M.M. Hanlon, A. Floudas, D.J. Veale, Cellular metabolic adaptations in rheumatoid arthritis and their therapeutic implications, *Nat. Rev. Rheumatol.* 18 (2022) 398–414.

- [36] F.P. Lafeber, W.H. Van der Laan, Progression of joint damage despite control of inflammation in rheumatoid arthritis: a role for cartilage damage driven synovial fibroblast activity, *Ann. Rheum. Dis.* 71 (2012) 793–795.
- [37] Y. Miao, et al., Contribution of ferroptosis and GPX4's dual functions to osteoarthritis progression, *EBioMedicine* 76 (2022), 103847.
- [38] X. Yao, et al., Chondrocyte ferroptosis contribute to the progression of osteoarthritis, *Journal of orthopaedic translation* 27 (2021) 33–43.
- [39] S. Mateen, S. Moin, A.Q. Khan, A. Zafar, N. Fatima, Increased reactive oxygen species formation and oxidative stress in rheumatoid arthritis, *PLoS One* 11 (2016), e0152925.
- [40] Y. Miyazaki, et al., G-type natriuretic peptide facilitates autonomic Ca(2+) entry in growth plate chondrocytes for stimulating bone growth, *Elife* 11 (2022).
- [41] S.A. Abiria, et al., TRPM7 senses oxidative stress to release Zn(2+) from unique intracellular vesicles, *Proc. Natl. Acad. Sci. U. S. A.* 114 (2017) E6079–E6088.
- [42] H.Y. Liang, et al., Immunomodulatory functions of TRPM7 and its implications in autoimmune diseases, *Immunology* 165 (2022) 3–21.
- [43] M. Aarts, et al., A key role for TRPM7 channels in anoxic neuronal death, *Cell* 115 (2003) 863–877.
- [44] H.S. Sun, et al., Suppression of hippocampal TRPM7 protein prevents delayed neuronal death in brain ischemia, *Nat. Neurosci.* 12 (2009) 1300–1307.
- [45] W. Nadolni, et al., TRPM7 kinase is essential for neutrophil recruitment and function via regulation of Akt/mTOR signaling, *Front. Immunol.* 11 (2020), 606893.
- [46] L. Pedrera, et al., Ferroptotic pores induce Ca(2+) fluxes and ESCRT-III activation to modulate cell death kinetics, *Cell Death Differ.* 28 (2021) 1644–1657.
- [47] D. Sarmiento, et al., Endotoxin-induced vascular endothelial cell migration is dependent on TLR4/NF-kappaB pathway, NAD(P)H oxidase activation, and transient receptor potential melastatin 7 calcium channel activity, *Int. J. Biochem. Cell Biol.* 55 (2014) 11–23.
- [48] B. Do Van, et al., Ferroptosis, a newly characterized form of cell death in Parkinson's disease that is regulated by PKC, *Neurobiol. Dis.* 94 (2016) 169–178.
- [49] J. Dachert, V. Ehrenfeld, K. Habermann, N. Dolgikh, S. Fulda, Targeting ferroptosis in rhabdomyosarcoma cells, *Int. J. Cancer* 146 (2020) 510–520.